International Journal of Nanomedicine

Dovepress
open access to scientific and medical research

Open Access Full Text Article

ORIGINAL RESEARCH

Paclitaxel/IR1061-Co-Loaded Protein Nanoparticle for Tumor-Targeted and pH/NIR-II-Triggered Synergistic Photothermal-Chemotherapy

This article was published in the following Dove Press journal:
International Journal of Nanomedicine

Li He[1,*]
Fangzhen Qing[2,*]
Maode Li[3]
Daitian Lan[3]

[1]Department of Thyroid and Breast Surgery, Sichuan Academy of Medical Sciences & Sichuan Provincial People's Hospital (East Hospital), Chengdu 610100, Sichuan, People's Republic of China; [2]Department of Stomatology, Sichuan Academy of Medical Sciences & Sichuan Provincial People's Hospital (East Hospital), Chengdu 610100, Sichuan, People's Republic of China; [3]Department of Hepatobiliary and Pancreatic Surgery, Sichuan Academy of Medical Sciences & Sichuan Provincial People's Hospital (East Hospital), Chengdu 610100, Sichuan, People's Republic of China

*These authors contributed equally to this work

Purpose: The aim of this study was to develop an "all-in-one" nanoplatform that integrates at the second near-infrared (NIR-II) region dye IR1061 and anticancer drug paclitaxel (PTX) into an apoferritin (AFN) nanocage (IR-AFN@PTX). Simultaneously, folic acid (FA), tumor target molecule, was conjugated onto IR-AFN@PTX to be IR-AFN@PTX-FA for tumor-targeted and pH/NIR-II-triggered synergistic photothermal-chemotherapy.

Methods: IR1061 was firstly reacted with PEG and then conjugated with AFN to be IR-AFN. Then, FA was conjugated onto the surface of IR-AFN to be IR-AFN-FA. At last, PTX was incorporated into IR-AFN-FA to fabricate a nanoplatform IR-AFN@PTX-FA. The NIR-II photothermal properties and pH/NIR-II triggered drug release were evaluated. The ability of IR-AFN@PTX-FA to target tumors was estimated using optical bioluminescence. In vitro and in vivo synergistic therapeutic effects of pH/NIR-II-triggered and tumor-targeted photothermal-chemotherapy were investigated in 4T1 tumor model.

Results: IR-AFN@PTX-FA showed excellent water solubility and physiological stability, which significantly enhanced the solubility of both IR1061 and PTX. After 5 min of laser irradiation at 1064 nm, IR-AFN@PTX-FA exhibited an effective photothermal effect compared with laser irradiation at 808 nm, even when blocked with 0.6 cm thick chicken breast. Cellular uptake experiments showed IR-AFN@PTX-FA utilized clathrin-mediated and caveolae-mediated endocytosis pathways to enter 4T1 cells, and was then delivered by the endosome to the lysosome. NIR-II laser irradiation and pH could synergistically trigger PTX release, inducing significant tumor inhibition in vitro and in vivo.

Conclusion: As a novel "all-in-one" nanoplatform, IR-AFN@PTX-FA was found to selectively target tumors and showed very efficient NIR-II photothermal effects and pH/NIR-II triggered drug release effects, showing a remarkable, synergistic photothermal-chemotherapy effect.

Keywords: IR1061, second near-infrared window, paclitaxel, apoferritin, "all-in-one" nanoplatform

Introduction

Nowadays, malignant tumors are among the most deadly diseases in the world. Surgical resection, radiation therapy and chemotherapy are the main clinical cancer treatments, although each of these therapies has drawbacks.[1–3] For example, surgical resection may lead to organ failure and rapid tumor metastasis; radiotherapy has toxic effects on normal tissues, and non-specific chemotherapy leads to severe systemic toxicity.[4–6] As a result, modern medical research has focused on the

Correspondence: Daitian Lan
Department of Hepatobiliary and Pancreatic Surgery, Sichuan Academy of Medical Sciences & Sichuan Provincial People's Hospital (East Hospital), Chengdu 610100, Sichuan, People's Republic of China
Tel +86-18349176311
Email doctor_yinl@126.com

submit your manuscript | www.dovepress.com
DovePress
http://doi.org/10.2147/IJN.S240707

urgent development of newer, less toxic treatment methods. In recent years, photothermal therapy (PTT) has been demonstrated as a highly effective cancer treatment by many scientists.[7–9] Photothermal reagents are designed to accumulate at tumor sites, and when the tumor sites are irradiated with near-infrared (NIR) lasers, site-specific hyperthermia is induced and the cancer cells die.[10,11] The laser is an important element in PTT, and its properties in biological tissues directly affect the therapeutic effect of PTT. Different wavelengths of lasers have different absorptions and scattering coefficients in biological tissues, affecting the penetration ability of the laser in tissues.[12–14] Therefore, the choice of laser wavelength is critical for tumor PTT.

At present, most PTT research uses lasers in the first near-infrared region (NIR-I) range, from 660 nm to 808 nm.[15,16] However, it has been reported that the NIR-I laser has strong absorption and can scatter in biological tissues, affecting its tissue penetrating ability, nor is it conducive to inducing hyperthermia of deep tumors or large solid tumors.[16,17] Some studies have found that lasers in the second NIR window (1000–1350 nm, NIR-II) have greater absorption and scatter less in biological tissue than those in the NIR I window, resulting in greater penetration and energy safety threshold.[18–20] The maximum allowable energy of the skin for an NIR-II laser is 1 W/cm^2, while for an NIR-I laser, the value is only 0.33 W/cm^2.[21] Therefore, the use of NIR-II PTT is an important breakthrough in achieving clinical safety and applicability. In addition, many studies report that there is often a deficiency in the use of a single therapy modality like PTT, including incomplete tumor suppression, which could lead to recurrence or metastasis.[22–24] Therefore, the use of NIR-II PTT combined with conventional chemotherapy represents a novel and promising treatment strategy. By combining a NIR-II photothermal reagent and anticancer drug with the same platform, hyperthermia and drug-specific delivery to the tumor area is achieved, thereby obtaining an effective synergistic tumor therapeutic effect.

NIR-II photothermal reagents include copper sulfide-based hybrid materials, gold nanostructures, silver nanoplates, carbon nanotubes and large conjugated polymer particles.[25–30] Although they demonstrate effective NIR-II PTT, biosafety is a major concern prior to clinical use. The IR1061 dye a commercial dye with high NIR-II (1064 nm) absorbance and low fluorescence quantum yield, and holds promise as a NIR-II photothermal agent but the hydrophobicity of IR1061 limits its use in biomedical applications.[31–33] In order to overcome this limitation, further modifications of the IR1061 are required.

Additionally, the use of a highly effective and low-toxic chemotherapy is essential for the treatment of tumors. At present, most anticancer drugs used in clinical practice are chemical synthetic drugs, such as doxorubicin and cisplatin, although treatment with these drugs are accompanied by serious side effects.[34,35] Paclitaxel (PTX) is an FDA-approved chemotherapy with fewer side effects and has a high inhibitory effect on a variety of malignant tumors.[36,37] However, its solubility in water is poor and requires delivery in a solution of Cremophor EL and ethanol for clinical use.[38] Cremophor EL has been reported to have serious side effects such as hypersensitivity reactions and acute renal impairment.[39,40]

In this study, we used pH-sensitive apoferritin (AFN) to carry IR1061 and PTX, and then modified the tumor target molecule folic acid (FA) to form a multifunctional, integrated NIR-II PTT and chemotherapy reagent (IR-AFN@PTX-FA). The carrier AFN is an iron-free spherical cage protein and is an excellent drug carrier with sensitivity to pH.[41–43] As the environment changes from acidic to alkaline, it can be reversibly denatured and reassembled.[44,45] Results show that IR-AFN@PTX-FA highly improves the water solubility of IR1061 and PTX and has excellent stability. In vitro and in vivo experiments show that IR-AFN@PTX-FA exhibits a high NIR-II photothermal effect, tumor specificity and tumor inhibition, and can be efficiently used for pH/NIR-II triggered synergistic photothermal-chemotherapy.

Materials and Methods

Materials

Horse spleen apoferritin (AFN) and fluorescein isothiocyanate (FITC) were from Sigma-Aldrich. Paclitaxel (PTX, ≥99%) was provided by Shanghai Jingchun Biotech Corporation. 1-ethyl-3-(3-dimethylaminopropyl) carbodiimide (EDC) and N-hydroxysuccinimide (NHS) were bought from Aladdin Bio-Chem Technology Co., LTD (Shanghai, China). FA-PEG$_{5000}$-NHS was obtained from Shanghai Ponsure Biotech. Co. Ltd. The functionalized poly(ethylene glycol) (SH-PEG5000-NH$_2$) was purchased from ToYongBio Tech. Inc. (Shanghai, China). Cell Counting Kit-8 (CCK-8) was obtained from Dojin Chemical Laboratory Co., Ltd.

Synthesis of IR-AFN@PTX-FA

One hundred milligram of SH-PEG5000-NH$_2$ and 50 mg of IR1061 were dissolved in 50 mL of dimethyl sulfoxide, and then reacted at room temperature for 36 hrs. The reaction

solvent was removed by distillation under reduced pressure, dissolving with deionized water. The unreacted PEG was then removed using a dialysis bag (MW: 7000 Da), and a brown compound (IR-PEG) was obtained by freeze-drying. Subsequently, IR-PEG and FA-PEG_{5000}-NHS (W/W = 2:1) were mixed and added to a 3 mg/mL AFN aqueous solution at presence of catalysts (15 mg of NHS and 25 mg of EDC) at room temperature for 36 hrs of reaction. After that, the mixture was dialyzed for 72 hrs (MW: 20,000 Da) to remove impurities. The final product (IR-AFN-FA) was further dried by freeze-drying to produce a solid powder. Next, water-insoluble PTX was dissolved in DMSO to be 2 mg/mL, and mixed with a 0.5 mg/mL IR-AFN-FA solution. The pH of the mixture was adjusted to less than 4.0 under 30 min of ultrasonication. After that, the pH of the mixture was slowly adjusted to 7.4, and dialyzed in distilled water overnight to remove free PTX molecules, resulting in the final product (IR-AFN@PTX-FA).

Characterization of IR-AFN@PTX-FA

The size and zeta potential of the samples were detected by a Zetasizer (Malvern, UK). The morphology of the samples was observed by a transmission electron microscope (TEM, Hitachi S-9300, Japan). FT-IR experiments were carried out by using Fourier Transform Infrared Spectroscopy (Bruker Tensor 27, Bruker Optik, Ettlingen, Germany) to detect the surface molecular structures. Fluorescence spectra were detected by a fluorescence spectrophotometer (Shimadzu EDX-GP, Japan). A commercial laser scanning microscope (LSM 510, Zeiss, Germany) was used to observe the fluorescence signal inside cells. Flow cytometry (FC500, Beckman Coulter) was used to quantitate the fluorescence intensity inside cells. The continued laser source at 808 nm and 1064 nm was from Beijing Laserwave Optoelectronics Technology Co. Ltd. Absorption spectra were detected by UV-VIS-NIR spectrophotometer (Cary 500, Varian Inc., CA, USA).

Study of NIR-II Photothermal Properties

In order to assess the NIR-II photothermal properties, we conducted a phantom experiment. In detail, IR-AFN @PTX-FA was mixed with agarose gel and placed under a 0.6 cm thick chicken breast. Then, the mixture was irradiated through the chicken breast with 808 nm and 1064 nm lasers of 0.75 W/cm^2, respectively, and the temperature was recorded after 5 mins. In addition, different concentrations of IR-AFN@PTX-FA solutions were placed in a 96-well plate and irradiated with a 1064 nm laser for 5 mins (0.75 W/cm^2). The temperature was recorded every 30 s and the thermal images were also captured using an infrared thermal camera (Fluke TI10, USA).

pH/NIR-II Triggered Drug Release

The pH/NIR-II triggered drug release was investigated according to previous papers.[44], 500 μL of IR-AFN@PTX-FA solution was placed in a D-tube (MWCO 8–12 kDa, Millipore) and the pH of solution was adjusted to 5.0 and 7.4. At the same time, at the different time point, the solution was irradiated by 1064 nm laser (0.75 W/cm^2) for 3 min and then 1 mL aliquots of dialysate were removed and replaced with 1 mL of fresh medium. The PTX release ratio was evaluated by a UV-VIS-NIR spectrophotometer.

Cell Lines

Mouse mammary tumor 4T1 cells and normal human breast cells MDA-kb2 were purchased from Chinese Academy of Sciences Cell Bank of Type Culture Collection (CBTCCCAS, Shanghai, China). The cells were cultured in complete DMEM media containing 10% fetal bovine serum, 89% DMEM and 1% penicillin–streptomycin at a humidified incubator (5% CO_2, 37°C).

Cellular Uptake Assay

According to literature reports,[36,44] FITC was used to label IR-AFN@PTX and IR-AFN@PTX-FA by physical adsorption. Treat 4T1 cells with FITC-labeled IR-AFN @PTX and IR-AFN@PTX-FA for 5 hrs, then stain with DAPI and lysosomal-specific dye LysoTracker, and observe IR-AFN@PTX and IR-AFN@PTX-FA in cells using commercial LSM. At the same time, intracellular fluorescence intensity was quantified using a flow cytometer. In addition, Bio-TEM is used to observe the intracellular nanoparticles.

To further study the cellular uptake mechanism of nanoparticles, we used a variety of endocytosis inhibitors (including 10 mM NaN_3, 10 μg/mL CPZ, and 10 μg/mL nystatin). In detail, 4T1 cells were seeded on a 96-well plate at a density of 5×10^4 cells/well, and cultured for 12 hrs. And then the above-mentioned endocytosis inhibitors were added. After 1 hr, remove the old culture medium, add FITC-labeled IR-AFN@PTX-FA (final concentration: 200 μg/mL), and incubate for further 3 hrs. The cells were then collected and the fluorescence intensity in the cells was measured by flow cytometry.

In vitro pH/NIR-II Triggered Photothermal-Chemotherapy

One hundred microlitersμL of 4T1 and MDA-kb2 cells suspension (1×10^4 cells/mL) was seeded into a 96-well plate. After 12 hrs of incubation, cells were treated with different concentrations of PTX formulation, IR-AFN@-FA, IR-AFN@PTX, IR-AFN@PTX-FA + FA (with the same PTX concentration) for 24 hrs. In addition, cells were treated with different concentrations of IR-AFN@-FA, IR-AFN@PTX, IR-AFN@PTX-FA + FA (with the same IR1061 concentration) for 24 hrs and 1064 nm laser irradiation (5 mins, 0.75 W/cm^2). Temperature changes and thermal images of the cells were recorded. The standard CCK-8 assay (Bestbio, China) was further used to assess the cytotoxicity. At the same time, these cells were co-stained with calcein-AM/PI (Aladdin, Shanghai, China) for 30 mins, and then imaged with a confocal laser scanning microscope (calcein-AM Ex = 488 nm, PI Ex = 535 nm).

Animal Model and in vivo Biodistribution

Balb/c nude mice (5–6 weeks old) were purchased from Charles River Laboratory (Beijing, China). To establish an animal 4T1 subcutaneous xenograft model, 150 μL of a cell suspension (10^6 cells) was injected subcutaneously into the backs of mice. Then, put it into the animal feeding room and observe the growth of the tumor. Tumor volume = length x width^2/2. All operations involving animal experiments strictly follow the guidelines for the care and use of laboratory animals of Sichuan Academy of Medical Sciences, which has been approved by the Animal Protection and Utilization Committee of Sichuan Academy of Medical Sciences.

In order to measure the circulating time of the nanoparticles in the blood, we injected free PTX and IR-AFN @PTX-FA (5 mg/kg PTX equivalent) into healthy Balb/c nude mice by intravenous injection (n = 5 per group). Then, the venous blood of the mice was collected at different time points and placed in a heparin-loaded blood collection tube. PTX was extracted from the plasma with an acidified isopropanol reagent, and its absorbance at 227 nm was measured to determine the concentration of PTX.

In addition, IR-AFN@PTX and IR-AFN@PTX-FA (100 μL) were injected into the tumor-bearing mice through the tail vein, and the main organs of the mice were detected at 0, 12, 24, and 36 hrs. The collected tissues were weighed, then digested with aqua regia, and finally the PTX content was detected by a UV-VIS-NIR spectrophotometer.

In vivo pH/NIR-II Triggered Photothermal-Chemotherapy

Prior to in vivo anticancer experiments, tumor-bearing mice were intravenously injected with saline, IR-AFN, IR-AFN @PTX and IR-AFN@PTX-FA (with same IR1061 concentration). After 24 hrs, the tumor was irradiated by 808 nm and 1064 nm laser (0.75 W/cm^2, 5 min), respectively. Additionally, the tumor region was covered with 0.6 cm thickness of chicken breast and then was irradiated by 808 nm and 1064 nm laser (0.75 W/cm^2, 5 min), respectively. The temperature and thermal images of the tumor region was recorded.

For in vivo photothermal-chemotherapy, tumor-bearing mice were randomly divided into six groups (n = 7): 1) PBS (100 μL); 2) PBS (100 μL) + NIR-II laser; 3) PTX formulation (100 μL, 4 mg/kg); 4) IR-AFN@PTX-FA (100 μL, 2 mg/kg); 5) IR-AFN@ PTX and 6) IR-AFN@PTX-FA (100 μL) + NIR-II laser. Twenty-four hours after the intravenous injection, the tumor area of the tumor-bearing mice in these groups was irradiated with a NIR-II laser (0.75 W/cm^2, 5 mins) once a day for 3 days. Tumor volume and body weight were recorded every 5 days during treatment. Relative tumor volume = V/V_0, where V_0 is the tumor volume when tumor treatment is started. In addition, for in vivo toxicity studies, healthy Balb/c mice were intravenously injected with 5 mg/kg and 10 mg/kg of IR-AFN@PTX-FA, respectively. After 35 days, major organs including lungs, heart, liver, spleen and kidneys were collected for histological analysis.

Statistical Analysis

All statistics are expressed as mean ± SD. Statistical significance was tested by two-tailed Student's *t*-test. $P < 0.05$ or $P < 0.01$ was considered statistically significant.

Results and Discussion

Synthesis and Characterization of IR-AFN@PTX-FA

The synthesis and bioapplication of IR-AFN@PTX-FA are shown in Figure 1. Commercial NIR-II dye IR1061 and tumor target molecule FA were conjugated onto the surface of apoferritin (AFN, iron-devoid spherical protein shell of ferritin). Subsequently, at low pH values less than 4, AFN disassembled the polypeptide subunits to encapsulate PTX, then the pH of the solution was slowly adjusted to approximately 7.4 to reassemble AFN and dialyzed to remove free PTX molecules. TEM showed that the IR-AFN@PTX-FA complex was a sphere with shell (Figure 2A), showing the polydispersion index (PDI) of 0.21, an average diameter of 35 nm and an average zeta potential of −30.9 mV (Figure 2B and C), as evaluated by a Nanosizer. Figure S1

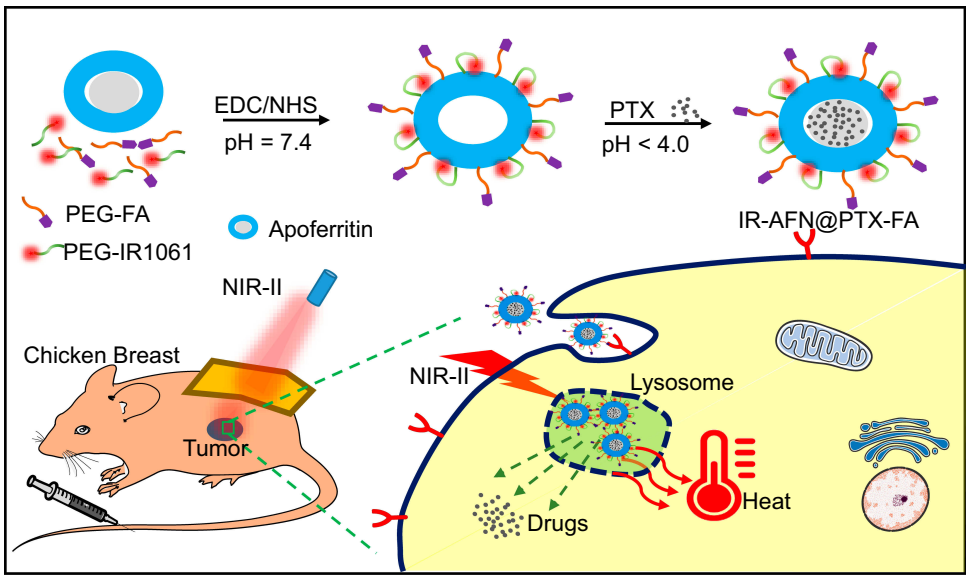

Figure 1 The schematic of preparation and application of IR-AFN@PTX-FA on tumor pH/NIR-II triggered photothermal-chemotherapy.
Abbreviations: TEM, transmission electron microscopy; IR, IR1061; AFN, apoferritin; PTX, paclitaxel; FA, folic acid; FBS, fetal bovine serum; PBS, phosphate buffer solution.

shows the FTIR spectrum of IR-AFN-FA. As seen in Figure S1, absorption bands at ~1106 cm^{-1} may correspond to the vibrational C-O-C ether linkage of PEG; absorption peaks at ~1650 cm^{-1} and ~1737 cm^{-1} belong to vibrational C=O bonds from PEG and AFN as well as from -COOH and -$CONH_2$ of FA and AFN; the bands at ~2859 cm^{-1}, ~2922 cm^{-1} and ~2970 cm^{-1} correspond to asymmetric and symmetric C-H stretch vibrations of -CH_2 of FA and PEG; absorption peaks at ~1455 cm^{-1} are associated to the phenyl ring of FA. The result confirms the successful conjugation of PEG, FA and AFN. Figure 2D demonstrates the spectra of IR1061 and

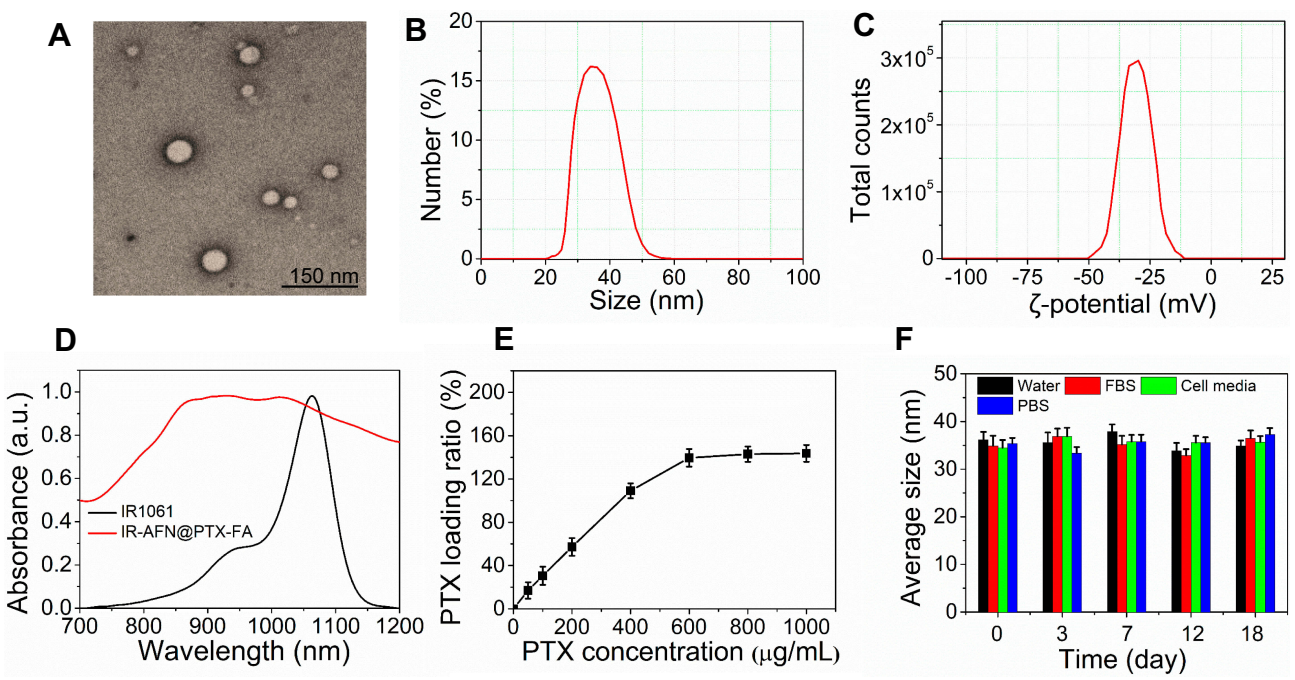

Figure 2 (**A**) The TEM image of IR-AFN@PTX-FA. (**B**) The size distribution and (**C**) zeta potential distribution of IR-AFN@PTX-FA. (**D**) The absorption spectra of IR1061 and IR-AFN@PTX-FA. (**E**) The PTX loading ratio of IR-AFN@PTX-FA. (**F**) The hydrodynamic particle size change of IR-AFN@PTX-FA in water, FBS, cell media PBS over 18 days.
Abbreviations: TEM, transmission electron microscopy; IR, IR1061; AFN, apoferritin; PTX, paclitaxel; FA, folic acid; FBS, fetal bovine serum; PBS, phosphate buffer solution.

IR-AFN@PTX-FA. IR-AFN@PTX-FA exhibited a broader NIR-II spectrum compared to free IR1061 (dissolved in DMSO), but still had high NIR-II absorbance at 1064 nm. As shown in Figure S2, the fluorescence spectra of free IR1061 and IR-AFN@PTX-FA were similar, indicating that the fluorescence properties of free IR1061 had no obvious change in IR-AFN@PTX-FA. The loading capacities of IR-AFN@PTX-FA increased with the increase of added PTX concentrations, and reached the highest PTX loading ratio of approximately 145.6% (Figure 2E). AFN is an iron-free spherical cage protein, assembled by the interaction of 24 polypeptide subunits which creates a spherical conformation with an external diameter of ~12 nm and an internal cavity of ~8 nm. As the environment changes from acidic to alkaline, it can be reversibly denatured and reassembled. Such an interesting pH-triggered assembly and disassembly behavior makes it a good candidate as drug delivery system to encapsulate chemotherapeutic drugs into its hollow cavity for cancer chemotherapy.[44,45] The high drug loading ratio was likely due to the large hollow cage structure of AFN. Figure 2F shows that the average size of IR-AFN@PTX-FA in water, FBS, cell media and PBS were similar over 18 days, suggesting that IR-AFN@PTX-FA shows a high stability, likely due to PEG conjugation and the nature of AFN.[44,45]

Study of NIR-II Photothermal Properties

Figure 3A shows a schematic illustration of the phantom experiment. The laser energy attenuation rate of 808 nm and 1064 nm lasers before and after penetration through the chicken breast tissue is shown in Figure 3B. As demonstrated, the 808 nm laser showed a higher attenuation rate than the 1064 nm laser. After 5 mins of irradiation, the IR-AFN@PTX-FA complex showed a temperature of 52.3°C under 1064 nm laser irradiation, which was significantly higher than the complex under 808 nm laser irradiation (38.2 °C) (Figure 3C). These results demonstrated that IR-AFN@PTX-FA covered with chicken breast tissue experiences a greater photothermal effect, with better tissue penetration under the 1064 nm laser compared to the 808 nm laser. This is likely due to less absorption and scattering in living tissue by the NIR-II laser compared to the NIR-I laser.[12,15,16] This demonstrates that the IR-AFN@PTX-FA complex, combined with 1064 nm laser is suitable for phototherapy in deep nidus.

pH/NIR-II-Triggered Drug Release

Figure 4A shows the schematic illustration of pH/NIR-II induced drug release and heat generation. As shown in Figure 4B, the temperature of the IR-AFN@PTX-FA solution was concentration-dependent, varying with different concentrations (0–200 μg/mL) at 1064 nm irradiation (0.75 W/cm^2, 5 min). The 200 μg/mL solution of IR-AFN@PTX-FA irradiated with NIR-II reached a maximum temperature of 63°C. Additionally, when the 200μg/mL IR-AFN@PTX-FA solution was irradiated under various laser strength it showed increased temperature with an increase in laser power (Figure 4C). Figure 4D shows thermal images of 200 ug/mL IR-AFN@PTX-FA following treatment with various laser strengths. After five cycles of NIR-II irradiation, IR-AFN@PTX-FA remained its initial photothermal effects (Figure 4E). Figure 4F shows the PTX release ratio in response to various pH and NIR-IIS irradiation conditions. The 24 hr release of PTX from IR-AFN@PTX-FA was only 3.2% at a physiological pH of 7.4, with a significant increase to 38.6% at pH 5.0. After six cycles of radiation (5 min, 1064 nm, 0.75 W/cm^2), 21.3% of PTX was released at pH 7.4, while 78.6% of PTX was released at pH 5.0 (Figure 4F), demonstrating that acidic conditions and photothermal could respectively induce PTX release. While the combination of acidic conditions and photothermal can synergistically promote PTX release.

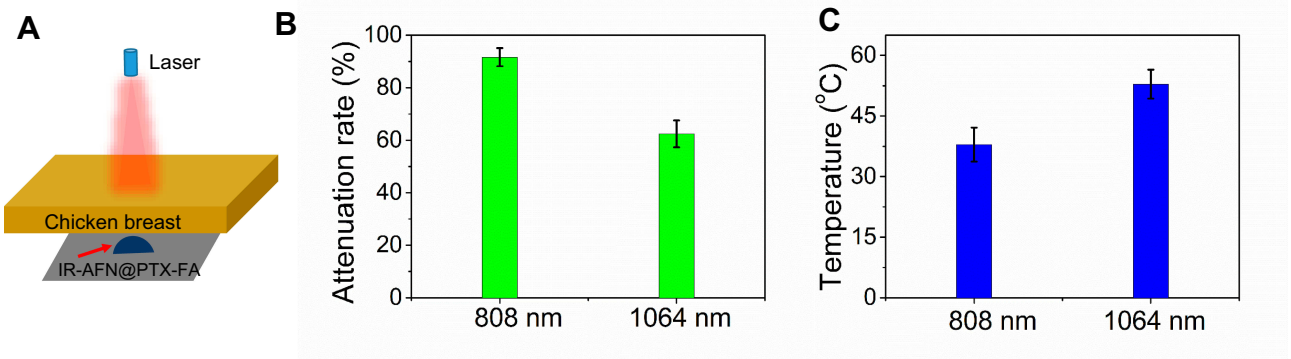

Figure 3 (**A**) The scheme of the phantom experiment. (**B**) The laser attenuation rate through a 0.6 cm thickness of chicken breast at 808 nm and 1064 nm wavelength, respectively. (**C**) The temperature of IR-AFN@PTX-FA beneath the chicken breast under 808 nm and 1064 nm laser irradiation.
Abbreviations: IR, IR1061; AFN, apoferritin; PTX, paclitaxel; FA, folic acid.

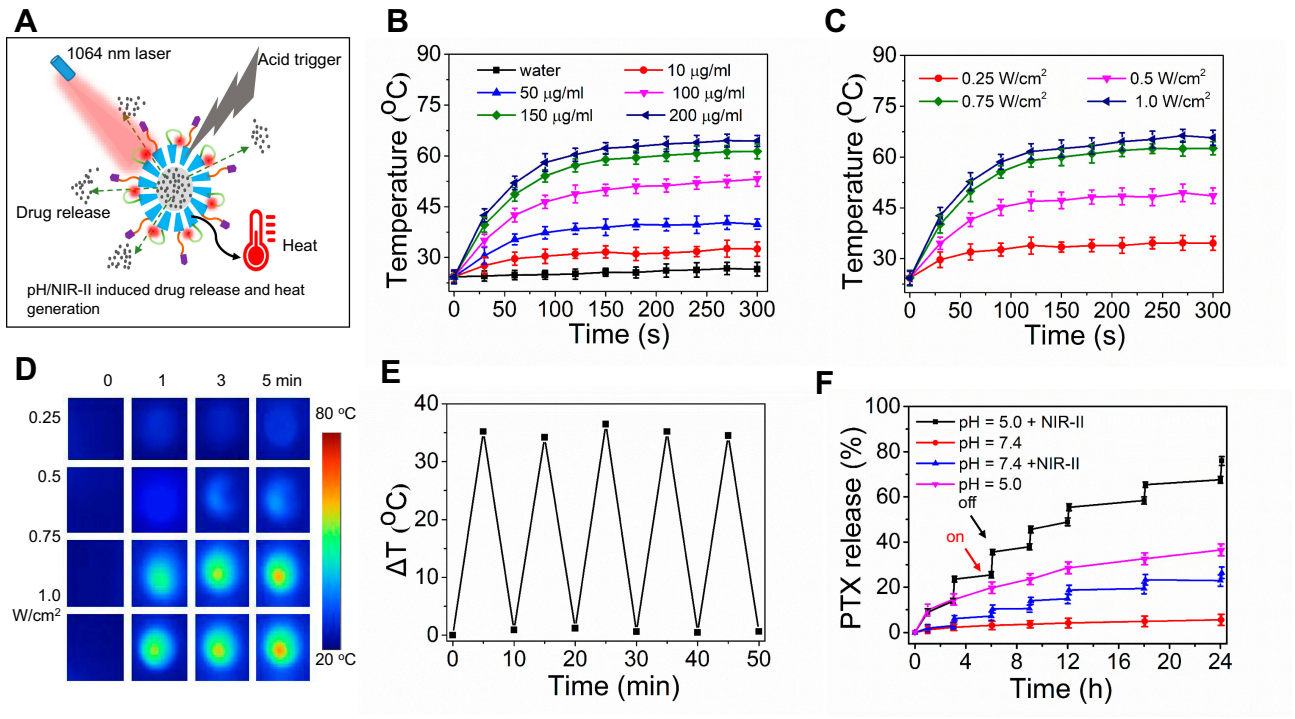

Figure 4 (**A**) The scheme of pH/NIR-II responded drug release and heat generation. (**B**) Photothermal heating curves of IR-AFN@PTX-FA solution at different concentrations under 5 min of 1064 nm laser irradiation (0.75 W/cm^2). (**C**) Photothermal heating curves and (**D**) thermal images of 200 ug/ml of IR-AFN@PTX-FA solution irradiated by different laser power density (under 5 min of 1064 nm laser irradiation). (**E**) Temperature variations (ΔT) of IR-AFN@PTX-FA after the continuous irradiations of 5 min of 1064 nm laser for 5 cycles. (**F**) Release kinetics of PTX from IR-AFN@PTX-FA in PBS buffer (pH = 7.4 and 5.0) with or without 1064 nm laser irradiation (0.75 W/cm^2).
Abbreviations: IR, IR1061; AFN, apoferritin; PTX, paclitaxel; FA, folic acid; NIR-II, second near infrared; PBS, phosphate buffer solution.

Acidic conditions can induce AFN disassembly and cage opening, and the addition of photothermal therapy accelerated the release of PTX from the cage. These findings provide further evidence for the application of IR-AFN@PTX-FA in tumor remotely controllable therapy.

Cellular Uptake

To assess the specificity of IR-AFN@PTX-FA, FITC was used as a fluorescent marker and conjugated to the nanoparticles to determine the kinetics of cellular uptake and the intracellular distribution of nanoparticles. Figure 5A shows the uptake ratio of FITC, IR-AFN@PTX, IR-AFN@PTX-FA and IR-AFN@PTX-FA + pretreatment with FA of 4T1 cells. These results indicated that the intracellular fluorescent intensity of IR-AFN@PTX-FA was markedly higher compared to the other treatments. It also confirmed the efficacy of improved cellular uptake and selectivity of FA modification in 4T1 tumor cells. Additionally, cellular uptake assay on normal human breast cells MDA-kb2 was also conducted, which were shown in Figure S3. As normal human breast cells are not FA high-expressed, the cell uptake ratio on IR-AFN@PTX and IR-AFN@PTX-FA groups showed no significant difference. The fluorescent images of the intracellular distribution of IR-AFN@PTX-FA are shown in Figure 5B. The majority of green fluorescence (IR-AFN@PTX-FA) overlapped with the red fluorescence (Lysotracker) and showed intense yellow fluorescence, indicating IR-AFN@PTX-FA is mainly located in the lysosome. TEM imaging shows the majority of IR-AFN@PTX-FA in endosomes or lysosome (Figure 5C). These data also demonstrated that the internalization of IR-AFN@PTX-FA occurred mainly via FA receptor-mediated endocytosis.

To further understand how tumor cells were taking up IR-AFN@PTX-FA, we quantitatively evaluated the effects of adenosine triphosphate (ATP) and other endocytic inhibitors on cellular uptake (Figure 5D). Pre-incubating with sodium azide (NaN_3), an ATP depleting reagent, significantly reduced the cellular uptake rate of IR-AFN@PTX-FA, indicating that IR-AFN@PTX-FA uptake by 4T1 cells is energy-dependent. In addition, the effect of temperature on cell uptake of IR-AFN@PTX-FA was also investigated. After incubating cells at 4°C with IR-AFN@PTX-FA, the cell uptake rate was reduced by 60% compared to the control group, suggesting that uptake of IR-AFN@PTX-FA requires active endocytosis. CPZ is a clathrin-coated pit-forming blocker that significantly reduced the uptake of IR-AFN

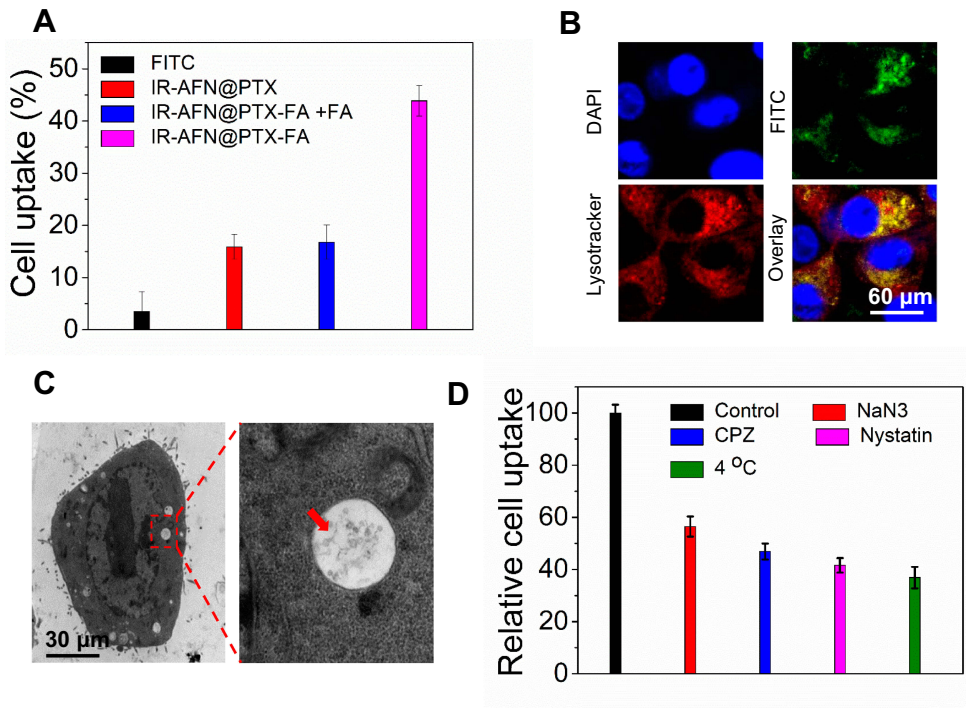

Figure 5 (**A**) Cell uptake ratio of free FITC, IR-AFN@PTX, IR-AFN@PTX-FA + FA, and IR-AFN@PTX-FA. (**B**) The fluorescence images of 4T1 cells incubated with FITC-labeled IR-AFN@PTX-FA for 3 h. Green fluorescence indicates the FITC signal, and red fluorescence indicates Lysotracker signal, yellow fluorescence indicates the overlay of green and red fluorescence. (**C**) The bio-TEM image of 4T1 cells after incubation with IR-AFN@PTX-FA for 3 h. (**D**) Investigation of the cellular internalization mechanism of IR-AFN@PTX-FA in 4T1 cells by using inhibitors of endocytosis. The internalization ratio was normalized to that of the control (IR-AFN@PTX-FA internalization without inhibitors).
Abbreviations: IR, IR1061; AFN, apoferritin; PTX, paclitaxel; FA, folic acid; TEM, transmission electron microscopy; FITC, fluorescein isothiocyanate; DAPI, 4',6-diamidino-2-phenylindole; CPZ, chlorpromazine.

@PTX-FA by 50%, indicating that the uptake of IR-AFN@PTX-FA by 4T1 cells is via clathrin-mediated endocytosis. In addition, nystatin, a caveolae disrupting agent, was used to pretreat cells, and showed an inhibitory effect on the uptake of IR-AFN@PTX-FA. These results indicate that the cellular uptake of IR-AFN@PTX-FA is through a clathrin-mediated active endocytosis mechanism.[46,47]

In vitro pH/NIR-II Triggered Photothermal-Chemotherapy

Figure 6A and B shows the temperature of 4T1 cells incubated with PBS, IR-AFN, IR-AFN@PTX and IR-AFN@PTX-FA (with same concentration of IR1061) following 1064 nm irradiation (0.75 W/cm^2) for 5 mins. The results showed that cells treated with IR-AFN@PTX-FA had the

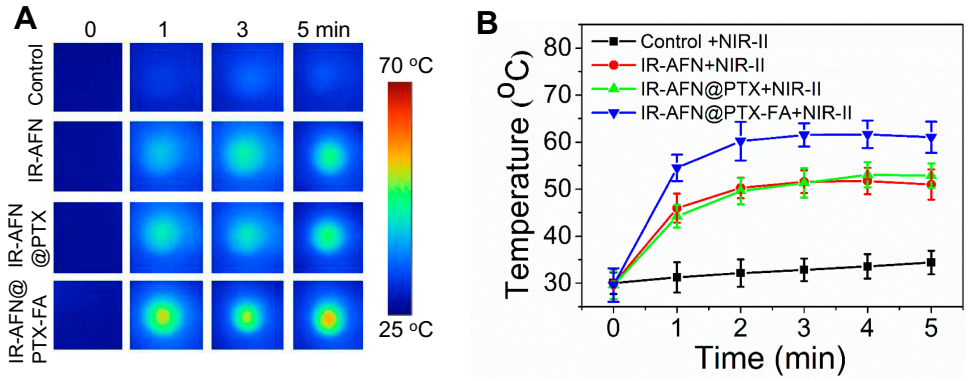

Figure 6 (**A**) Thermal images and (**B**) the corresponding temperature change curves of control, IR-AFN, IR-AFN@PTX, IR-AFN@PTX-FA treated cells in 96-well plates after 5 min of 1064 nm laser irradiation (0.75 W/cm^2).
Abbreviations: IR, IR1061; AFN, apoferritin; PTX, paclitaxel; FA, folic acid; NIR-II, second near infrared.

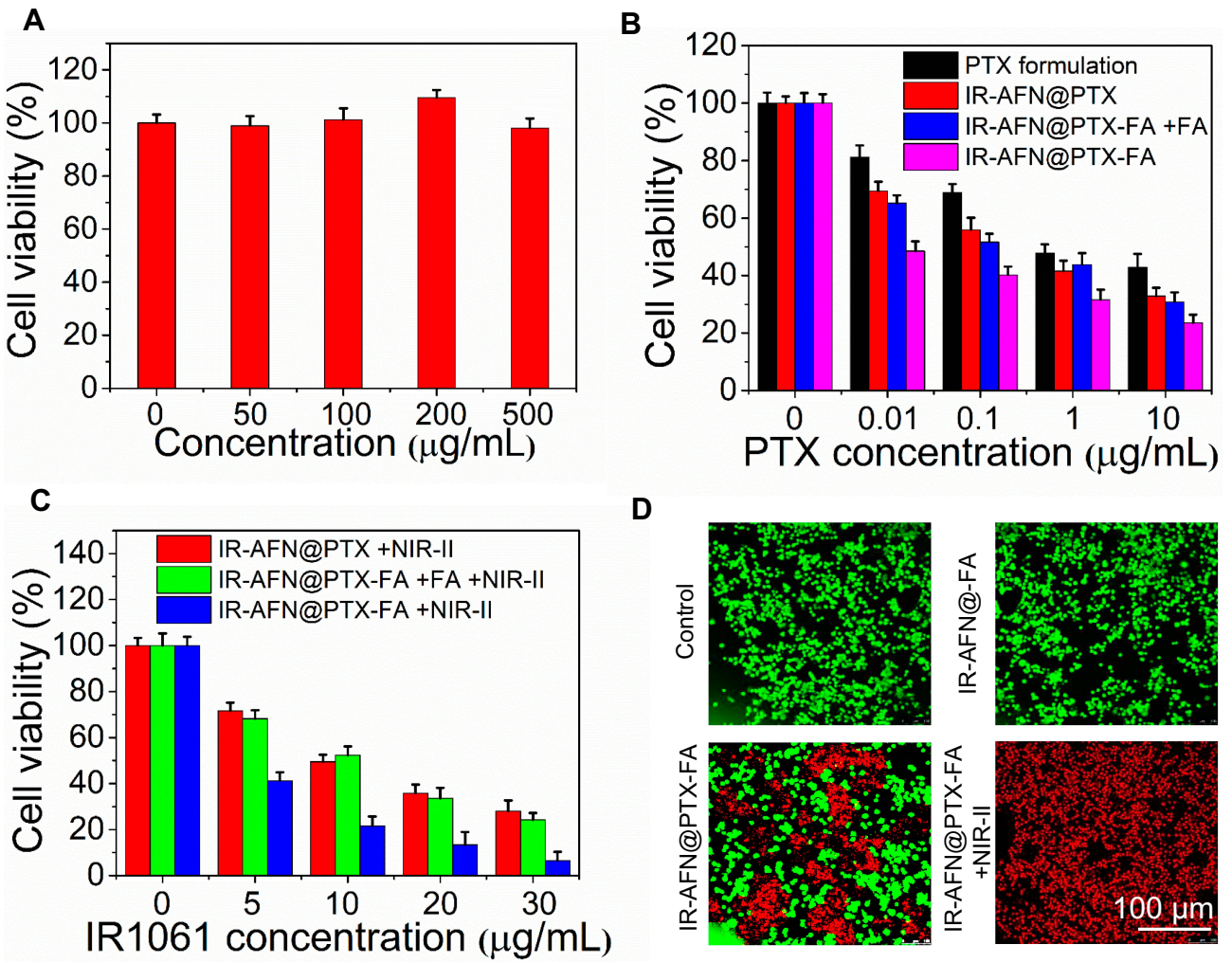

Figure 7 (**A**) Cell viability of 4T1 cells treated with different concentration of IR-AFN-FA. (**B**) Cell viability of 4T1 cells treated with various concentrations of PTX formulation, IR-AFN@PTX, IR-AFN@PTX-FA and IR-AFN@PTX-FA + FA pretreatment (at the same PTX concentration). (**C**) Cell viability of 4T1 cells treated with various concentrations of IR-AFN@PTX, IR-AFN@PTX-FA and IR-AFN@PTX-FA + FA pretreatment (at the same IR1061 concentration) with 1064 nm laser irradiation (5 min, 0.75 W/cm^2). (**D**) The calcium AM/PI dual-staining images of cells after treatment with control (PBS), IR-AFN@-FA, IR-AFN@PTX-FA, IR-AFN@PTX-FA +NIR-II, respectively.
Abbreviations: IR, IR1061; AFN, apoferritin; PTX, paclitaxel; FA, folic acid; NIR-II, second near infrared; PBS, phosphate buffer solution; PI, propidium iodide; calcium AM, 3',6'-Di(O-acetyl)-4',5'-bis[N,N-bis(carboxymethyl)aminomethyl]fluorescein, tetraacetoxymethyl ester.

highest temperature increase (ΔT = 22°C) compared to PBS, IR-AFN, or IR-AFN@PTX, likely due to the high cellular uptake of IR-AFN@PTX-FA, with that temperature increase far exceeding the temperature that cells can survive at. The cytotoxicity of IR-AFN-FA on 4T1 and MDA-kb2 cells was evaluated with a CCK-8 assay (Figure 7A and Figure S4), showing that IR-AFN-FA at a concentration up to 0.5 mg/mL did not significantly decrease viability. This suggests that IR-AFN-FA as a vehicle for PTX is biocompatible for both tumor and normal human breast cells. The 4T1 and MDA-kb2 cells were also treated with various concentrations of PTX formulation, IR-AFN@PTX, IR-AFN@PTX-FA and IR-AFN@PTX-FA + FA pretreatment (at the same PTX concentration), showing a concentration-dependent decrease in cell viability (Figure 7B). Among these groups, the IR-AFN@PTX-FA at all tested concentrations displayed the greatest inhibitory effect on proliferation. In contrast, various concentrations of IR-AFN@PTX, IR-AFN@PTX-FA and IR-AFN@PTX-FA + FA pretreatment (at the same IR1061 concentration) combined with NIR-II laser treatment (0.75 W/cm^2, 5 min) showed the greatest effect on cell death (Figure 7C). Among these groups, IR-AFN@PTX-FA at all concentrations also displayed the greatest inhibitory effect on cell proliferation with a 93% viability inhibition ratio in the 30 ug/mL + NIR-II laser-treated group. While on MDA-kb2 cells, IR-AFN@PTX-FA combined with or without NIR-II showed similar cell viability inhibition (Figure S4), likely due to the normal cells had low cell uptake ratio. Calcein-AM

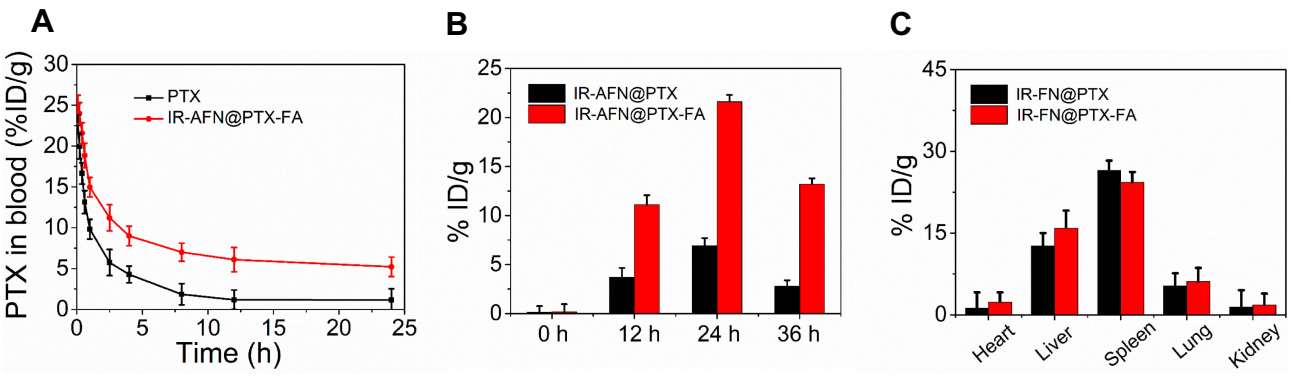

Figure 8 (**A**) The blood circulation time of free PTX and IR-AFN@PTX-FA in healthy mice. (**B**) The content of IR-AFN@PTX and IR-AFN@PTX-FA in tumor tissue at different time points post-injection. (**C**) The content of IR-AFN@PTX and IR-AFN@PTX-FA in major organs including heart, liver, spleen, lung and kidney at 24 h post-injection.
Abbreviations: IR, IR1061; AFN, apoferritin; PTX, paclitaxel; FA, folic acid.

/PI dual staining was used to investigate the cytotoxic effect of IR-AFN@PTX-FA with or without NIR-II laser irradiation. PBS and IR-AFN@-FA treated cells exhibited no red fluorescence (dead cells). Some cells treated with IR-AFN @PTX-FA without NIR-II laser were dead, and a combination of that treatment with NIR-II laser irradiation resulted in almost complete cell death (Figure 7D). These results showed that IR-AFN@PTX-FA combined with NIR-II laser treatment showed a remarkable and synergistic effect on cell viability, where FA targeting promoted the internalization of IR-AFN@PTX-FA, generating more heat upon NIR-II irradiation and releasing more PTX.

In vivo pH/NIR-II Triggered Photothermal-Chemotherapy

As shown in Figure 8A, the length of time that IR-AFN @PTX-FA could be detected in the blood circulation of healthy mice was longer compared to free PTX, which can be ascribed to the PEG modification.[44,48] The increased time in circulation time facilitated the accumulation of IR-AFN @PTX-FA at the tumor site. Additionally, after intravenous injection into tumor-bearing mice, IR-AFN@PTX-FA exhibited higher accumulation than IR-AFN@PTX (Figure 8B) and reached a peak at 24 h post-injection, likely attributing to its ability to remain in the blood circulation for a longer period and FA targeting effect. In addition to tumor accumulation, IR-AFN@PTX-FA also accumulated in the liver and spleen at 24 h post-injection (Figure 8C), suggesting that the nanoparticles may be metabolized at these sites.

As shown in Figure 9A and B, at 24 hrs post-injection and after 5 mins of 808 nm and 1064 nm laser irradiation, the temperature of tumors irradiated with the 1064 nm laser was significantly higher than that by 808 nm in all nanoparticle-treated groups. This was due to the higher absorbance of IR-AFN@PTX-FA at 1064 nm than at 808 nm, with the 1064 nm laser also having deeper tissue penetration than the 808 nm laser. In order to confirm this result, we covered the tumor region with a 0.6 cm thick piece of chicken breast, and irradiated the area with the 808 nm and 1064 nm lasers. As shown in Figure 9C, after 5 min irradiation, IR-AFN@PTX-FA treated tumor-bearing mice exhibited a 15°C increase with 1064 nm laser irradiation, and only a 6°C increase with 808 nm laser irradiation. The result verified the deeper tissue penetration of the 1064 nm laser.

In order to study the photothermal-chemotherapy effect in vivo, the nanoparticles were injected via tail vein into tumor-bearing mice and irradiated with or without NIR-II laser irradiation daily for 3 days. As shown in Figure 9D, control with or without NIR-II irradiation exhibited no tumor suppression, groups treated with the PTX formulation, IR-AFN@PTX-FA, IR-AFN@PTX + NIR-II showed no completed inhibition of tumor growth. As expected, the group treated with IR-AFN@PTX-FA exhibited significant suppression of tumor growth. During the treatment, the body weight did not decrease significantly (Figure 9E), indicating that the injection dose did not affect overall mouse health. Healthy Balb/c mice were intravenously injected with IR-AFN@PTX-FA (5 or 10 mg/kg), and major organs, including lung, heart, liver, spleen, and kidney, were harvested for histological analysis after 35 days. As shown in Figure 9F, there was no noticeable organ damage visible on H&E staining. Taken together, these findings illustrate that the IR-AFN@PTX-FA complex induced a synergistic photothermal-chemotherapy effect, ascribing to FA targeting, the NIR-II photothermal effect and PTX remote-controllable triggered release by with a pH/NIR-II dual-stimulus.[49–51]

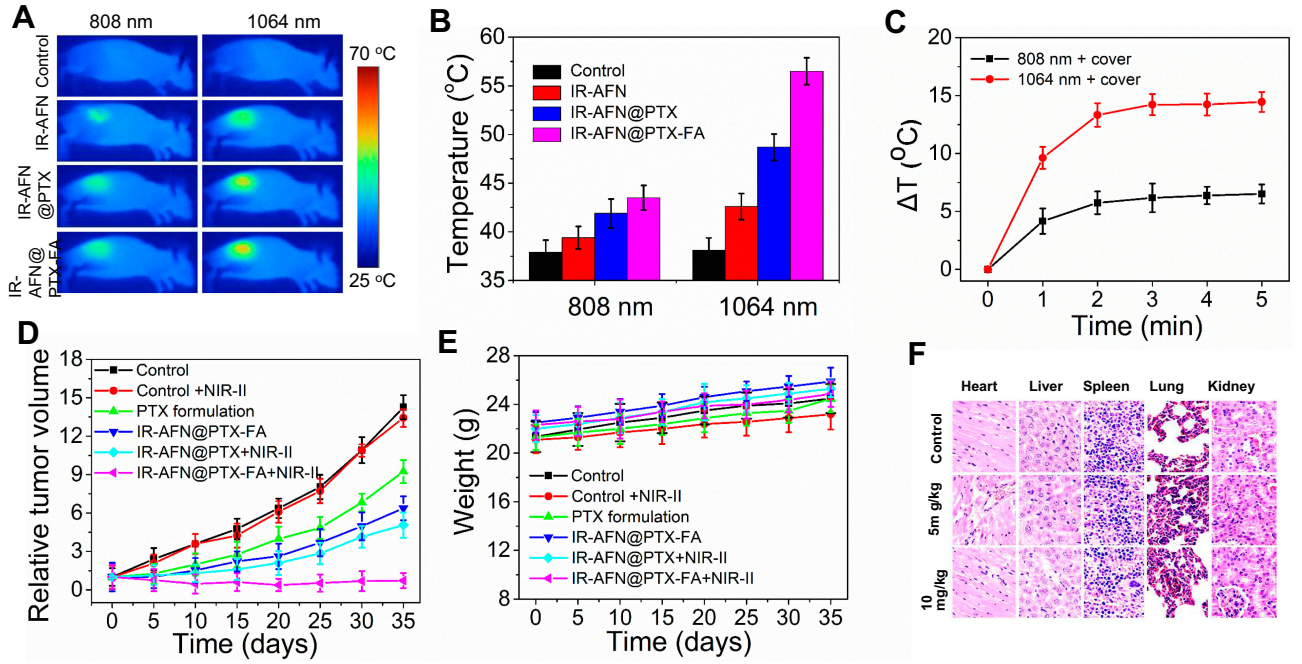

Figure 9 (**A**) The thermal images and (**B**) corresponding temperature statistical results of tumor bearing mice post tail vein injection of PBS, IR-AFN, IR-AFN@PTX and IR-AFN@PTX-FA at 24 h under 5 min of 808 nm and 1064 nm laser irradiation (0.75 W/cm^2), respectively. (**C**) The temperature change (ΔT) of IR-AFN@PTX-FA covered by chicken breast under 808 nm and 1064 nm laser irradiation. (**D**) The growth profile of 4T1 xenografted tumors after intravenous injection of control, control + NIR-II, PTX formulation, IR-AFN@PTX-FA, IR-AFN@PTX + NIR-II and IR-AFN@PTX-FA+ NIR-II. (**E**) Body weight of tumor-bearing mice after intravenous injection of control, control + NIR-II, PTX formulation, IR-AFN@PTX-FA, IR-AFN@PTX + NIR-II and IR-AFN@PTX-FA+ NIR-II. (**F**) H&E images of major organs of mice treated with 5 mg/kg and 10 mg/kg for 35 days, respectively. Magnification: ×200.

Abbreviations: IR, IR1061; AFN, apoferritin; PTX, paclitaxel; FA, folic acid; NIR-II, second near infrared; PBS, phosphate buffer solution; H&E, hematoxylin and eosin.

Conclusion

In this study, we present an "all-in-one" nanoplatform IR-AFN@PTX-FA that possesses selectivity to target tumors, shows a substantial NIR-II photothermal and pH/NIR-II triggered drug release effect, applied in the setting of tumor photothermal-chemotherapy. Combining IR1061 and PTX into the IR-AFN@PTX-FA complex significantly enhanced the solubility of these individual reagents, and the entire complex demonstrated excellent water solubility and physiological stability. IR-AFN@PTX-FA could be reached beneath chicken breast tissue, showing strong photothermal effects after 5 min of 1064 nm laser irradiation, compared with 808 nm laser irradiation. IR-AFN@PTX-FA was also taken up easily and in high quantity by 4T1 cells, which utilized both clathrin-mediated and caveolae-mediated endocytosis pathways to enter cells and showed distribution in the lysosome. NIR-II laser irradiation and pH could synergistically and intensely trigger PTX release, inducing significant tumor inhibition in vitro and in vivo. Biosafety evaluation showed IR-AFN@PTX-FA has no significant systematic toxicity. These findings demonstrate that the IR-AFN@PTX-FA holds great promise as an effective NIR-II synergistic photothermal-chemotherapy agent to treat large solid tumors or tumor in deep tissue.

Author Contributions

All authors contributed to data analysis, drafting or revising the article, gave final approval of the version to be published, and agree to be accountable for all aspects of the work.

Disclosure

The authors report no conflicts of interest in this study.

References

1. Badwe R, Hawaldar R, Nair N, et al. Locoregional treatment versus no treatment of the primary tumour in metastatic breast cancer: an open-label randomised controlled trial. *Lancet Oncol*. 2015;16(13):1380–1388. doi:10.1016/S1470-2045(15)00135-7
2. Curigliano G, Burstein HJ, P Winer E, et al. De-escalating and escalating treatments for early-stage breast cancer: the St. Gallen international expert consensus conference on the primary therapy of early breast cancer 2017. *Ann Oncol*. 2017;28(8):1700–1712. doi:10.1093/annonc/mdx308
3. Khorana AA, Mangu PB, Berlin J, et al. Potentially curable pancreatic cancer: American Society of Clinical Oncology clinical practice guideline. *J Clin Oncol*. 2016;34(21):2541–2556. doi:10.1200/JCO.2016.67.5553

4. Petteys RJ, Spitz SM, Goodwin CR, et al. Factors associated with improved survival following surgery for renal cell carcinoma spinal metastases. *Neurosurg Focus*. 2016;41(2):E13. doi:10.3171/2016.5.FOCUS16145
5. Yock TI, Yeap BY, Ebb DH, et al. Long-term toxic effects of proton radiotherapy for paediatric medulloblastoma: a Phase 2 single-arm study. *Lancet Oncol*. 2016;17(3):287–298. doi:10.1016/S1470-2045(15)00167-9
6. Xin Y, Huang Q, Tang JQ, et al. Nanoscale drug delivery for targeted chemotherapy. *Cancer Lett*. 2016;379(1):24–31. doi:10.1016/j.canlet.2016.05.023
7. Doughty ACV, Hoover AR, Layton E, et al. Nanomaterial applications in photothermal therapy for cancer. *Materials*. 2019;12(5):779. doi:10.3390/ma12050779
8. Wang H, Chang J, Shi M, Pan W, Li N, Tang B. A dual-targeted organic photothermal agent for enhanced photothermal therapy. *Angew Chem Int Ed Engl*. 2019;58(4):1057–1061. doi:10.1002/anie.201811273
9. Chen J, Li X, Liu X, et al. Hybrid $MoSe_2$–indocyanine green nanosheets as a highly efficient phototheranostic agent for photoacoustic imaging guided photothermal cancer therapy. *Biomater Sci*. 2018;6(6):1503–1516. doi:10.1039/c8bm00104a
10. Vankayala R, Hwang KC. Near-infrared-light-activatable nanomaterial-mediated phototheranostic nanomedicines: an emerging paradigm for cancer treatment. *Adv Mater*. 2018;30(23):1706320. doi:10.1002/adma.201706320
11. Jung HS, Verwilst P, Sharma A, Shin J, Sessler JL, Kim JS. Organic molecule-based photothermal agents: an expanding photothermal therapy universe. *Chem Soc Rev*. 2018;47(7):2280–2297. doi:10.1039/c7cs00522a
12. Jacques SL. Optical properties of biological tissues: a review. *Phys Med Biol*. 2013;58(11):R37–R61. doi:10.1088/0031-9155/58/11/R37
13. Zhang H, Salo DC, Kim DM, et al. Penetration depth of photons in biological tissues from hyperspectral imaging in shortwave infrared in transmission and reflection geometries. *J Biomed Opt*. 2016;21(12):126006. doi:10.1117/1.JBO.21.12.126006
14. Salehpour F, Cassano P, Rouhi N, et al. Penetration profiles of visible and near-infrared lasers and light-emitting diode light through the head tissues in animal and human species: a review of literature. *Photobiomodul Photomed Laser Surg*. 2019;37(10):581–595. doi:10.1089/photob.2019.4676
15. Chen G, Zhang Y, Li C, Huang D, Wang Q, Wang Q. Recent advances in tracking the transplanted stem cells using near-infrared fluorescent nanoprobes: turning from the first to the second near-infrared window. *Adv Healthc Mater*. 2018;7(20):e1800497. doi:10.1002/adhm.201800497
16. Zhao J, Zhong D, Zhou S. NIR-I-to-NIR-II fluorescent nanomaterials for biomedical imaging and cancer therapy. *J Mater Chem B*. 2018;6(3):349–365. doi:10.1039/C7TB02573D
17. Wan H, Yue J, Zhu S, et al. A bright organic NIR-II nanofluorophore for three-dimensional imaging into biological tissues. *Nature Commun*. 2018;9(1):1171. doi:10.1038/s41467-018-03505-4
18. Vijayaraghavan P, Liu CH, Vankayala R, Chiang CS, Hwang KC. Designing multi-branched gold nanoechinus for NIR light activated dual modal photodynamic and photothermal therapy in the second biological window. *Adv Mater*. 2014;26(39):6689–6695. doi:10.1002/adma.201400703
19. Wang X, Ma Y, Sheng X, Wang Y, Xu H. Ultrathin polypyrrole nanosheets via space-confined synthesis for efficient photothermal therapy in the second near-infrared window. *Nano Lett*. 2018;18(4):2217–2225. doi:10.1021/acs.nanolett.7b04675
20. Yang T, Tang Y, Liu L, et al. Size-dependent Ag_2S nanodots for second near-infrared fluorescence/photoacoustics imaging and simultaneous photothermal therapy. *ACS Nano*. 2017;11(2):1848–1857. doi:10.1021/acsnano.6b07866
21. Lu W, Melancon MP, Xiong C, et al. Effects of photoacoustic imaging and photothermal ablation therapy mediated by targeted hollow gold nanospheres in an orthotopic mouse xenograft model of glioma. *Cancer Res*. 2011;71(19):6116–6121. doi:10.1158/0008-5472.CAN-10-4557
22. Huang Q, Wang S, Zhou J, Zhong X, Huang Y. Albumin-assisted exfoliated ultrathin rhenium disulfide nanosheets as a tumor targeting and dual-stimuli-responsive drug delivery system for a combination chemo-photothermal treatment. *RSC Adv*. 2018;8(9):4624–4633. doi:10.1039/C7RA13454A
23. Kuthala N, Vankayala R, Li YN, Chiang CS, Hwang KC. Engineering novel targeted boron-10-enriched theranostic nanomedicine to combat against murine brain tumors via MR imaging-guided boron neutron capture therapy. *Adv Mater*. 2017;29(31):1700850. doi:10.1002/adma.201700850
24. Ayala-Orozco C, Urban C, Bishnoi S, et al. Sub-100 nm gold nanomatryoshkas improve photo-thermal therapy efficacy in large and highly aggressive triple negative breast tumors. *J Control Release*. 2014;191:90–97. doi:10.1016/j.jconrel.2014.07.038
25. Wang Z, Huang P, Jacobson O, et al. Biomineralization-inspired synthesis of copper sulfide–ferritin nanocages as cancer theranostics. *ACS Nano*. 2016;10(3):3453–3460. doi:10.1021/acsnano.5b07521
26. Ku G, Zhou M, Song S, Huang Q, Hazle J, Li C. Copper sulfide nanoparticles as a new class of photoacoustic contrast agent for deep tissue imaging at 1064 nm. *ACS Nano*. 2012;6(8):7489–7496. doi:10.1021/nn302782y
27. Li J, Jiang R, Wang Q, et al. Semiconducting polymer nanotheranostics for NIR-II/Photoacoustic imaging-guided photothermal initiated nitric oxide/photothermal therapy. *Biomaterials*. 2019;217:119304. doi:10.1016/j.biomaterials.2019.119304
28. Huang X, Tang S, Liu B, Ren B, Zheng N. Enhancing the photothermal stability of plasmonic metal nanoplates by a core-shell architecture. *Adv Mater*. 2011;23(30):3420–3425. doi:10.1002/adma.201100905
29. Welsher K, Sherlock SP, Dai H. Deep-tissue anatomical imaging of mice using carbon nanotube fluorophores in the second near-infrared window. *Proc Natl Acad Sci U S A*. 2011;108(22):8943–8948. doi:10.1073/pnas.1014501108
30. Cao Y, J H D, Zhao N, et al. Highly efficient NIR-II photothermal conversion based on an organic conjugated polymer. *Chem Mater*. 2016;29(2):718–725. doi:10.1021/acs.chemmater.6b04405
31. Xie X, Hu Y, Zhang C, Song J, Zhuang S, Wang Y. A targeted biocompatible organic nanoprobe for photoacoustic and near-infrared-II fluorescence imaging in living mice. *RSC Adv*. 2019;9(1):301–306. doi:10.1039/C8RA08163H
32. Li J, Pu K. Development of organic semiconducting materials for deep-tissue optical imaging, phototherapy and photoactivation. *Chem Soc Rev*. 2019;48(1):38–71. doi:10.1039/c8cs00001h
33. Chen Q, Chen J, He M, et al. Novel small molecular dye-loaded lipid nanoparticles with efficient near-infrared-II absorption for photoacoustic imaging and photothermal therapy of hepatocellular carcinoma. *Biomater Sci*. 2019;7(8):3165–3177. doi:10.1039/c9bm00528e
34. Galsky MD, Pal SK, Chowdhury S, et al. Comparative effectiveness of gemcitabine plus cisplatin versus methotrexate, vinblastine, doxorubicin, plus cisplatin as neoadjuvant therapy for muscle-invasive bladder cancer. *Cancer*. 2015;121(15):2586–2593. doi:10.1002/cncr.29387
35. Wu H, Jin H, Wang C, et al. Synergistic cisplatin/doxorubicin combination chemotherapy for multidrug-resistant cancer via polymeric nanogels targeting delivery. *ACS Appl Mater Interfaces*. 2017;9(11):9426–9436. doi:10.1021/acsami.6b16844
36. Deng W, Qiu J, Wang S, et al. Development of biocompatible and VEGF-targeted paclitaxel nanodrugs on albumin and graphene oxide dual-carrier for photothermal-triggered drug delivery in vitro and in vivo. *Int J Nanomedicine*. 2018;13:439–453. doi:10.2147/IJN.S150977

37. Xiao K, Luo J, Fowler WL, et al. A self-assembling nanoparticle for paclitaxel delivery in ovarian cancer. *Biomaterials*. 2009;30(30):6006–6016. doi:10.1016/j.biomaterials.2009.07.015
38. Zhang C, Lu T, Tao J, Wan G, Zhao H. Co-delivery of paclitaxel and indocyanine green by PEGylated graphene oxide: a potential integrated nanoplatform for tumor theranostics. *RSC Adv*. 2016;6(19):15460–15468. doi:10.1039/C5RA25518J
39. Gogaté US, Schwartz PA, Agharkar SN. Effect of unpurified cremophor EL on the solution stability of paclitaxel. *Pharm Dev Technol*. 2009;14(1):1–8. doi:10.1080/10837450802409354
40. Kim SC, Kim DW, Shim YH, et al. In vivo evaluation of polymeric micellar paclitaxel formulation: toxicity and efficacy. *J Control Release*. 2001;72(1–3):191–202. doi:10.1016/S0168-3659(01)00275-9
41. Breen AF, Wells G, Turyanska L, Bradshaw TD. Development of novel apoferritin formulations for antitumour benzothiazoles. *Cancer Rep*. 2019;2(4):e1155. doi:10.1002/cnr2.1155
42. Ghosh S, Mohapatra S, Thomas A, et al. Apoferritin nanocage delivers combination of microtubule and nucleus targeting anticancer drugs. *ACS Appl Mater Interfaces*. 2016;8(45):30824–30832. doi:10.1021/acsami.6b11798
43. Dostalova S, Vasickova K, Hynek D, et al. Apoferritin as an ubiquitous nanocarrier with excellent shelf life. *Int J Nanomedicine*. 2017;12:2265–2278. doi:10.2147/IJN.S130267
44. Zheng Q, Cheng W, Zhang X, Shao R, Li Z. A pH-induced reversible assembly system with resveratrol-controllable loading and release for enhanced tumor-targeting chemotherapy. *Nanoscale Res Lett*. 2019;14(1):305. doi:10.1186/s11671-019-3139-z
45. Zhang Q, Chen J, Shen J, et al. Inlaying radiosensitizer onto the polypeptide shell of drug-loaded ferritin for imaging and combinational chemo-radiotherapy. *Theranostics*. 2019;9(10):2779–2790. doi:10.7150/thno.33472
46. Qian J, Xu N, Zhou X, et al. Low density lipoprotein mimic nanoparticles composed of amphipathic hybrid peptides and lipids for tumor-targeted delivery of paclitaxel. *Int J Nanomedicine*. 2019;14:7431–7446. doi:10.2147/IJN.S215080
47. Dalal C, Saha A, Jana NR. Nanoparticle multivalency directed shifting of cellular uptake mechanism. *J Phys Chem C*. 2016;120(12):6778–6786. doi:10.1021/acs.jpcc.5b11059
48. Xin Y, Liu T, Yang C. Development of PLGA-lipid nanoparticles with covalently conjugated indocyanine green as a versatile nanoplatform for tumor-targeted imaging and drug delivery. *Int J Nanomedicine*. 2016;11:5807. doi:10.2147/IJN.S119999
49. Xie J, Mei L, Huang K, et al. A photo-inducible protein–inorganic nanoparticle assembly for active targeted tumour theranostics. *Nanoscale*. 2019;11(13):6136–6144. doi:10.1039/C9NR01120J
50. Xie J, Lu Y, Wang W, et al. Simple protein modification using zwitterionic polymer to mitigate the bioactivity loss of conjugated insulin. *Adv Healthc Mater*. 2017;6(11):1601428. doi:10.1002/adhm.201601428
51. Xie J, Li Y, Cao Y, et al. Photo synthesis of protein-based drug-delivery nanoparticles for active tumor targeting. *Biomater Sci*. 2013;1(12):1216–1222. doi:10.1039/C3BM60174A